Spin-dependent nonlocal resistance in a Si/SiGe quantum Hall conductor

K. Hamaya,* K. Sugihara, H. Takahashi, S. Masubuchi, M. Kawamura, and T. Machida†
Institute of Industrial Science, University of Tokyo, 4-6-1 Komaba, Meguro-ku, Tokyo 153-8505, Japan

K. Sawano and Y. Shiraki
Research Center for Silicon Nano-Science, Advanced Research Laboratories, Musashi Institute of Technology, 8-15-1 Todoroki, Setagaya-ku, Tokyo 158-0082, Japan

(Received 5 October 2006; revised manuscript received 3 November 2006; published 12 January 2007)

We study the edge-channel transport at quantum Hall (QH) transition regions for a high-mobility Si/SiGe QH conductor by measuring nonlocal resistance (R_{NL}). The R_{NL} as a function of magnetic field changes drastically after Landau-level crossings. The features of the R_{NL} depend on the spin configuration between the innermost edge channel and the bulk state: the R_{NL} appears only when the relevant edge-bulk states have opposite spin orientations. Also, an origin of the spin-dependent resistivity [Phys. Rev. Lett. **94**, 176402 (2005)] at QH transition regions is discussed in terms of the spin-dependent inter-edge-bulk scattering.

DOI: 10.1103/PhysRevB.75.033307 PACS number(s): 73.43.−f

In a perpendicular high magnetic field, the energy spectrum of a two-dimensional electron system (2DES) splits into discrete quantized energies, Landau levels (LLs). When the magnetic field is tilted from the normal to the 2DES plane, the Zeeman splitting (ΔE_z) is enhanced with increasing parallel magnetic component ($B_{\parallel}$) in addition to the normal component ($B_{\perp}$), leading to a Landau-level crossing, which is the so-called coincidence. Using this coincidence method, one can examine the correlation between magnetotransport and the spin configuration of the relevant LLs. In 2DESs confined to AlAs quantum wells, Vakili *et al.*[1] recently discovered the spin-dependent resistivity at the transition region between integer quantum Hall (QH) states before and after coincidence conditions: enhancement of the resistivity can be seen when the spin orientation of the partially filled LL was aligned with the majority spin. A similar spin-dependent resistivity was also observed in high-mobility Si/SiGe heterostructures.[2] The above two studies claimed that the spin-dependent resistivity originates from a screening effect of the Coulomb interaction from the low-lying filled LLs. In the QH regime, on the other hand, the importance of edge-channel transport has been indicated,[3–5] and it was suggested that scattering events between edge channels are related to the spin configuration of the relevant edge channels.[6,7] Recently, using a coincidence method, we experimentally demonstrated the strong spin dependence of the inter-edge-channel scattering event in a Si/SiGe QH device.[8] Since adiabatic edge-channel transport affects the magnetotransport properties even at QH transition regions,[9,10] we need to pay attention to the effect of the spin configuration of the relevant edge and bulk states on edge-channel transport to clarify the origin of the spin-dependent resistivity which is a recent topic in dispute.[1,2]

In this report, we study the adiabatic edge-channel transport at QH transition regions for a high-mobility Si/SiGe heterostructure. The nonlocal resistance (R_{NL}), which is a conventional tool to directly detect the inter-edge-bulk (IEB) scattering rate, depends strongly on the spin configuration between the innermost edge channel and the bulk state: the R_{NL} is experimentally observed only when the relevant edge-bulk states have opposite spin orientations. Also, we find that the variation in the R_{NL} amplitude is opposite to that in the longitudinal resistance (R_{xx}) amplitude before and after the coincidences. A possible origin of the spin-dependent resistivity discovered by Vakili *et al.*[1] at QH transition regions is the spin-dependent IEB scattering.

We study a high-mobility $Si/Si_{0.75}Ge_{0.25}$ heterostructure grown by molecular beam epitaxy (MBE) on a strained-relaxed $Si_{0.75}Ge_{0.25}$ buffer layer smoothed by chemical mechanical polishing (CMP).[11] The wafer has an electron mobility of 41 $m^2/V\,s$ and electron density of 1.96×10^{15} m^{-2} at 50 mK, and was patterned into 40-μm-wide Hall bars with alloyed AuSb Ohmic contacts as shown in the inset of Fig. 1(b). Transport measurements were performed using standard lock-in techniques (18 Hz) with various alternating cur-

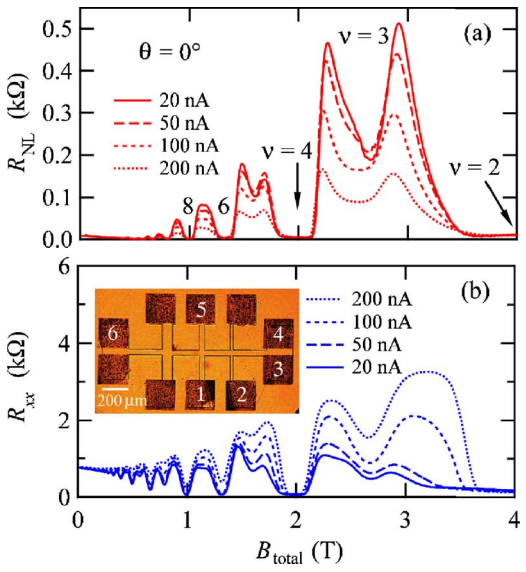

FIG. 1. (Color online) (a) Nonlocal resistance ($R_{NL}=R_{15,23}$) and (b) longitudinal resistance ($R_{xx}=R_{46,21}$) as a function of external magnetic field for various measurement currents. The inset shows the optical micrograph of the Hall bar sample, and the numbers used in the measurements are depicted.

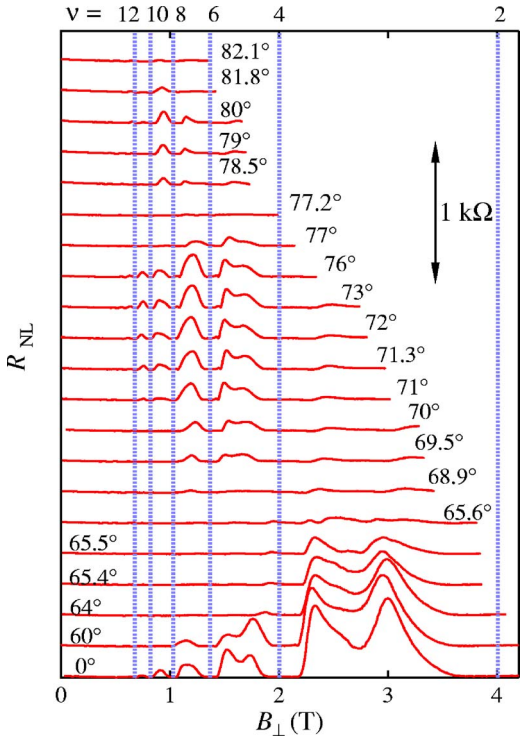

FIG. 2. (Color online) (a) The R_{NL}-$B_{\perp}$ curves measured at various θ. The blue dashed lines indicate the plateau center of the QH states, and the LL filling factors are marked on the top. All the data are measured at I_{ac}=20 nA.

rents (I_{ac}) in a ^{3}He-^{4}He dilution refrigerator at 50 mK.

Figure 1 shows (a) nonlocal resistance (R_{NL}) and (b) longitudinal resistance (R_{xx}) as a function of total magnetic field (B_{total}) for various currents I_{ac} of 20, 50, 100, and 200 nA. The R_{NL} and R_{xx} are defined as $R_{15,23}=V_{23}/I_{15}$ and $R_{46,21}=V_{21}/I_{46}$, respectively, as shown in the inset of Fig. 1(b). The plateaus at filling factors of Landau levels, $\nu=2,6,10,\ldots$ and $\nu=4,8,12,\ldots$, are attributed to Zeeman splitting and cyclotron energy gaps, respectively. Also, the dip structures shown at odd integer filling factors of $\nu=3$ and 5 are derived from valley splitting. Classically, the V_{23}/I_{15} ($=R_{15,23}$) cannot emerge because the current path is far from the voltage probes. In Fig. 1(a), however, the R_{NL} as a function of B_{total} is clearly observed with significant I_{ac} dependence at the transition regions between QH states. These are the first observations of the R_{NL} for Si-based QH systems. The observed R_{NL} in Fig. 1(a) indicates the presence of adiabatic edge-channel transport at transition regions in the Si/SiGe QH conductor. A similar adiabatic transport over macroscopic lengths has already been observed in high-mobility AlGaAs/GaAs QH conductors,[9,10] in which the R_{NL} arises from suppression of the electron scattering between the innermost edge channel and the bulk state.[9,10] Here we regard two valley-induced edge channels as one degenerated edge channel. With increasing I_{ac}, the IEB scattering is accelerated, leading to a decrease in the amplitude of the R_{NL}. An evident current dependence of Shubnikov–de Haas oscillations (R_{xx}-B_{total} curves) is also seen in Fig. 1(b), and the oscillations are significantly grown with increasing I_{ac}, which are caused by an acceleration of the IEB scattering. We note

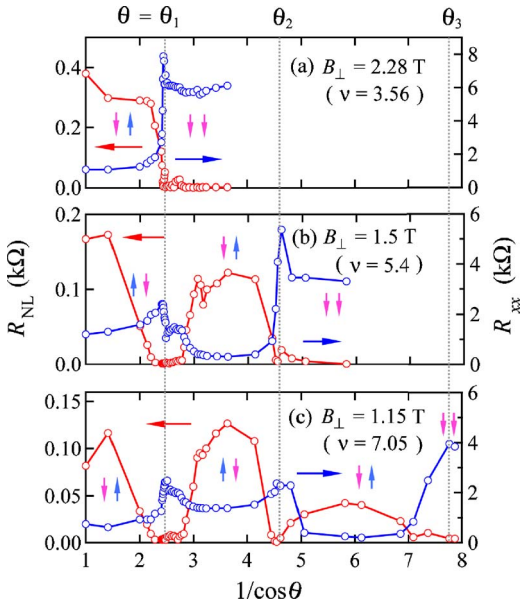

FIG. 3. (Color online) Plots of the R_{NL} (left axis) and the R_{xx} (right axis) vs $1/\cos\theta$ for $B_{\perp}$= (a) 2.28 T, (b) 1.5 T, and (c) 1.15 T. The gray dashed lines correspond to the first, second, and third coincidence angles θ_1, θ_2, and θ_3. The spin orientations of the innermost edge channel and the bulk state are depicted.

that the current dependence of the R_{xx} is opposite to that of the R_{NL}.

To explore the change in the IEB scattering before and after coincidences, we measure the angular-dependent R_{NL}. Figure 2 shows the R_{NL}-$B_{\perp}$ curves for various values of θ, where θ is defined as an angle between the direction normal to the 2DES plane and the direction of an applied magnetic field.[12] The measured data are recorded at I_{ac}=20 nA. The first, second, and third coincidence angles θ_1, θ_2, and θ_3, were deduced by measuring R_{xx} for different θ: θ_1=65.6°, θ_2=77.5°, and θ_3=82.6°.[13–15] After the first coincidence, the signal from the R_{NL} disappears once in $65.6° \lesssim \theta \lesssim 68.9°$ in all over the $B_{\perp}$ range. Although we can see wiggles and very small peaks, we checked that these features have no current dependence: these data are not related to the R_{NL} with the current dependence which was observed in Fig. 1(a). These features probably originate from the field dependence of R_{xx} component due to the sample geometry used. For the following findings, we have already examined the above current dependence to judge whether these are R_{NL} components or not. In $69.5° \lesssim \theta \lesssim 77.0°$, the R_{NL} appears again whereas no signal from the R_{NL} in $2<\nu<4$ can be seen. Also, near the second coincidence angle ($\theta \sim 77.2°$), the R_{NL} vanishes again, but we can see the small peaks from the R_{NL} in $6<\nu<10$ in $78.5° \lesssim \theta \lesssim 81.8°$, together with no R_{NL} signal in $4<\nu<6$. With further increasing θ, we observed no signal from the R_{NL} once again in $82.1° \lesssim \theta \lesssim 83.2°$. Though a very small signal from the R_{NL} in $10<\nu<12$ was detected at θ =83.1° and θ=83.3°, we could not obtain it at θ=83.6°.

Figure 3 shows the plots of the R_{NL} (red) and R_{xx} (blue) as a function of $1/\cos\theta$ ($=B_{total}/B_{\perp}$) for various $B_{\perp}$. First, we focus on the R_{NL} vs $1/\cos\theta$ for the representative $B_{\perp}$ with a R_{NL} peak. At $B_{\perp}$=2.28 T (ν=3.56), a finite R_{NL} decreases

abruptly down to ~0 at around θ_1. This means that the QH state collapses at coincidence conditions, where one cannot distinguish the edge channels and the bulk state. It should be noted that, in $\theta_1 < \theta < \theta_2$, the R_{NL} remains zero even after the coincidence. For $B_\perp = 1.5$ T ($\nu = 5.4$), on the other hand, the R_{NL} can be seen again in $\theta_1 < \theta < \theta_2$, indicating that the IEB scattering is suppressed. In $\theta_2 < \theta < \theta_3$, however, the R_{NL} disappears again, being similar to that seen in $\theta_1 < \theta < \theta_2$ for $B_\perp = 2.28$ T. For $B_\perp = 1.15$ T ($\nu = 7.05$), the R_{NL} can be observed even in $\theta_2 < \theta < \theta_3$, but the R_{NL} vanishes in $\theta_3 < \theta$.

From the data, we can find the R_{NL}—that is, suppression of the IEB scattering—depends strongly on the coincidence events. In order to comprehend the features gained in Fig. 3, we illustrate (a) the energy level diagrams and (b) the representative dispersion diagrams of edge and bulk states at QH transition regions in Fig. 4. In $0° < \theta < \theta_1$, the spin orientations of the edge channel and the inner bulk state always become opposite when the Fermi level is located in the transition regions between QH states as shown in Fig. 4(a). In contrast, the spin configuration of (edge channel, bulk state) in $2 < \nu < 4$ is switched from (↓, ↑) to (↓, ↓) after the first coincidence ($\theta_1 < \theta < \theta_2$), induced by the enhancement in ΔE_z. After the second coincidence ($\theta_2 < \theta < \theta_3$), spin switching also occurs in $4 < \nu < 6$, and the similar switching can be expected in $6 < \nu < 8$ after the third coincidence ($\theta_3 < \theta$). In this context, it can be inferred that the observed disappearance of the R_{NL} for $B_\perp = 2.28$ T in $\theta_1 < \theta < \theta_2$, 1.5 T in $\theta_2 < \theta < \theta_3$, and 1.15 T in $\theta_3 < \theta$ is related to the spin configuration of the relevant edge and bulk states. For example, we pay attention to the $4 < \nu < 6$ transition region and the schematic dispersion diagrams in Fig. 4(b). After the second coincidence ($\theta_2 < \theta < \theta_3$), the spin configuration between the innermost edge channel and the bulk state is varied from (↓, ↑) to (↓, ↓); that is, the spin orientations become the same, while the spin orientations are opposite after the first coincidence ($\theta_1 < \theta < \theta_2$) in spite of the spin switching. Here we return to the data for $B_\perp = 1.5$ T ($\nu = 5.4$) in Fig. 3 where the R_{NL} did not appear after the second coincidence ($\theta_2 < \theta < \theta_3$). In this regard, we review that the effect of spin configuration on the R_{NL}. When the spin orientations of the edge and bulk states are the same—e.g., (↓, ↓)—the IEB scattering is likely to be accelerated. The same interpretation can be adapted for the data for $B_\perp = 2.28$ T ($\nu = 3.56$) and $B_\perp = 1.15$ T ($\nu = 7.05$). The other transition regions—e.g., $8 < \nu < 10$, etc.—showed the same features qualitatively.

In AlGaAs/GaAs systems,[5] the scattering between the innermost edge channel and the bulk state is governed by their spatial separation, ΔX. In particular, the ΔX of the spin-resolved levels is based on the ΔE_z; as a result, the IEB scattering can be generally suppressed as the ΔX is expanded by the enhancement in the ΔE_z. In the present case, when the θ is raised and the first coincidence occurs, the ΔX becomes the maximum derived from the cyclotron energy gap of $\hbar\omega_c$. However, the R_{NL} cannot be seen with increasing θ in $2 < \nu < 4$. In short, the edge-bulk scattering events cannot be explained only by the change in the ΔX. Hence, we should deliberate the spin configuration in the relevant edge-bulk states in order to interpret the features observed in Fig. 3. Recently, we experimentally demonstrated that the inter-

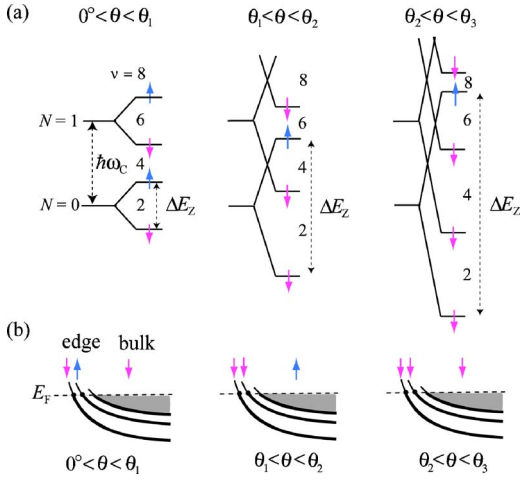

FIG. 4. (Color online) (a) Energy-level diagrams of electrons for $0° < \theta < \theta_1$, $\theta_1 < \theta < \theta_2$, and $\theta_2 < \theta < \theta_3$ in the single-particle picture for Si/SiGe QH systems. (b) Energy dispersion diagrams of the relevant edge and bulk states in $4 < \nu < 6$ for various θ.

edge-channel (IEC) scattering depends merely on the spin orientation between the relevant edge channels in a Si/SiGe QH device.[8] The R_{NL} discussed here depends on the spin configuration of the edge and bulk states, as well as the edge-edge scattering reported previously.[6–8] We now infer that the suppression of the IEB scattering originates from the restriction of the spin-flip scattering processes, caused by the weak spin-orbit interaction in Si systems.[8]

We in turn concentrate on the R_{xx} as a function of $1/\cos\theta$ in Fig. 3. For $B_\perp = 2.28$ T ($\nu = 3.56$) the R_{xx} increases significantly at around θ_1, which is a general feature around coincidence conditions.[13–15] After the first coincidence ($\theta_1 < \theta < \theta_2$), the R_{xx} shows a constant value of ~6 kΩ. Also, for $B_\perp = 1.5$ T ($\nu = 5.4$) and $B_\perp = 1.15$ T ($\nu = 7.05$), similar saturation behavior of the R_{xx} can be seen after the second and third coincidences ($\theta_2 < \theta < \theta_3$ and $\theta_3 < \theta$), respectively. The saturated R_{xx} after the increase has already been reported in AlAs quantum wells in Fig. 2 of Ref. 1, and this has been considered as the spin-dependent resistivity due to screening effect of the Coulomb interaction from the filled LLs.[1,2] We notice that the R_{NL} discussed above vanishes with the saturation of the R_{xx} when the spin orientations of the low-lying LLs are the same in regard to the partially filled level in which the Fermi energy resides. Taking this inverse dependence and the current dependence shown in Fig. 1 into account, we can deduce that the R_{xx} features presented here are dominated by the IEB scattering event. Namely, with regard to the spin-dependent resistivity discovered by Vakili *et al.*,[1] our experimental data in Fig. 3 indicate the clear influence of the IEB scattering of electrons on the R_{xx}: when the R_{xx} is suppressed, the R_{NL} appears, while when the R_{xx} is enhanced, the R_{NL} disappears, systematically. As is well known, since the IEB scattering depends on the magnitude of the current flow,[9] the complicated current dependence of the IEB scattering also becomes crucial. In fact, although the spin-dependent R_{xx} similar to the data reported by Lai *et al.*[2] was observed at $I_{ac} = 20$ nA after the first coincidence, the spin

dependence was broken by increasing I_{ac} for our samples (not shown here). Accordingly, the spin dependence of the R_{NL} presented in this paper—i.e., the spin-dependent suppression of the IEB scattering—influences the R_{xx} at transition regions in QH systems.

In summary, we have studied a nonlocal resistance due to the suppression of the inter-edge-bulk scattering of electrons for a high-mobility Si/SiGe quantum Hall system. We have found an evident dependence of the nonlocal resistance on the spin configurations of the relevant edge-bulk regions. Also, the spin-dependent resistivity discovered by Vakili *et al.*[1] at QH transition regions can be probed by measuring the nonlocal resistance.

This work is supported by PRESTO, JST Agency, a Grant-in-Aid from MEXT (No. 17244120), the Special Coordination Funds for Promoting Science and Technology, and the Iketani Science and Technology Foundation. K.H. acknowledges support from the JSPS Research Program for Young Scientists.

*Electronic mail: hamaya@iis.u-tokyo.ac.jp
†Electronic mail: tmachida@iis.u-tokyo.ac.jp

[1] K. Vakili, Y. P. Shkolnikov, E. Tutuc, N. C. Bishop, E. P. De Poortere, and M. Shayegan, Phys. Rev. Lett. **94**, 176402 (2005).
[2] K. Lai, T. M. Lu, W. Pan, D. C. Tsui, S. Lyon, J. Liu, Y. H. Xie, M. Mühlberger, and F. Schäffler, Phys. Rev. B **73**, 161301(R) (2006).
[3] M. Büttiker, Phys. Rev. B **38**, 9375 (1988).
[4] R. J. Haug, A. H. MacDonald, P. Streda, and K. von Klitzing, Phys. Rev. Lett. **61**, 2797 (1988).
[5] S. Komiyama, H. Hirai, M. Ohsawa, Y. Matsuda, S. Sasa, and T. Fujii, Phys. Rev. B **45**, 11085 (1992).
[6] G. Müller, D. Weiss, A. V. Khaetskii, K. von Klitzing, S. Koch, H. Nickel, W. Schlapp, and R. Lösch, Phys. Rev. B **45**, R3932 (1992).
[7] A. V. Khaetskii, Phys. Rev. B **45**, R13777 (1992).
[8] K. Hamaya, S. Masubuchi, K. Hirakawa, S. Ishida, Y. Arakawa, K. Sawano, Y. Shiraki, and T. Machida, Phys. Rev. B **73**, 121304(R) (2006).
[9] S. Komiyama, H. Nii, M. Ohsawa, S. Fukatsu, Y. Shiraki, R. Itoh, and H. Toyoshima, Solid State Commun. **80**, 157 (1991); S. Komiyama and H. Nii, Physica B **184**, 7 (1993).
[10] P. L. McEuen, A. Szafer, C. A. Richter, B. W. Alphenaar, J. K. Jain, A. D. Stone, R. G. Wheeler, and R. N. Sacks, Phys. Rev. Lett. **64**, 2062 (1990).
[11] K. Sawano, S. Koh, Y. Shiraki, Y. Hirose, T. Hattori, and K. Nakagawa, Appl. Phys. Lett. **82**, 412 (2003).
[12] The direction of the magnetic field rotation is parallel to the long axis of the Hall bar sample, where the large R_{xx} peak can be observed at $\nu=4$ as reported in Ref. 15.
[13] P. Weitz, R. J. Haug, K. von Klitzing, and F. Schäffler, Surf. Sci. **361-362**, 542 (1996).
[14] S. J. Koester, K. Ismail, and J. O. Chu, Semicond. Sci. Technol. **12**, 384 (1997).
[15] U. Zeitler, H. W. Schumacher, A. G. M. Jansen, and R. J. Haug, Phys. Rev. Lett. **86**, 866 (2001); U. Zeitler, H. W. Schumacher, J. Regul, R. J. Haug, P. Weitz, A. G. M. Jansen, and F. Schäffler, Physica E (Amsterdam) **6**, 288 (2000).